Efficient inverted polymer solar cells employing favourable molecular orientation

Varun Vohra,[a]* Kazuaki Kawashima,[b,c] Takeshi Kakara,[c] Tomoyuki Koganezawa,[d] Itaru Osaka,[b,e]* Kazuo Takimiya,[b]* Hideyuki Murata[a]*

[a] School of Materials Science, Japan Advanced Institute of Science and Technology (JAIST), 1-1 Asahidai, Nomi, Ishikawa, 923-1292, Japan

[b] Emergent Molecular Function Research Group, RIKEN Center for Emergent Matter Science (CEMS), Wako, Saitama 351-0198, Japan

[c] Department of Applied Chemistry, Graduate School of Engineering, Hiroshima University, 1-4-1 Kagamiyama, Higashi-Hiroshima, Hiroshima 739-8527, Japan

[d] Japan Synchrotron Radiation Research Institute, 1-1-1 Kouto, Sayo-cho, Sayo-gun, Hyogo 679-5198, Japan

[e] Precursory Research for Embryonic Science and Technology, Japan Science and Technology Agency, Chiyoda-ku, Tokyo 102-0075, Japan

E-mail: varun.vohra@uec.ac.jp (V.V.), itaru.osaka@riken.jp (I.O.), takimiya@riken.jp (K.T.), murata-h@jaist.ac.jp (H.M.)

Present address for V.V: Department of Engineering Science, Graduate School of Informatics and Engineering, The University of Electro-Communications (UEC), 1-5-1 Chofugaoka Chofu-shi Tokyo Japan, 182-8585

Abstract.

The improvement in the power conversion efficiency is a critical issue for polymer-based bulk-heterojunction solar cells (PSCs). Here, we show that high efficiencies of ~10% can be obtained by using a crystalline polymer, PNTz4T, in single-junction inverted cells with the thick active layer measuring ca. 300 nm. The improved performance is likely due to the large population of the polymer crystallites with the face-on orientation and the "favourable" distribution of edge-on and face-on crystallites along the film thickness, as revealed by in-depth studies of the blend films using grazing incidence wide angle X-ray diffraction, which results in the reduction of charge recombination and the efficient charge transport. These results underscore the great promise of PSCs, and raise hopes of achieving even higher efficiencies by materials development and control of molecular ordering.

Bulk-heterojunction (BHJ) solar cells consisting of semiconducting polymers and fullerene derivatives as the p-type (hole transport or electron donor) and n-type (electron transport or electron acceptor) materials, respectively, is an emerging device that enables light-weight, large-area, flexible, low-cost, and low-energy fabrication, in contrast to the silicon technology.[1-3] Although the power conversion efficiency (PCE) of such polymer-based BHJ solar cells (PSCs) has rapidly improved in the last decade, exceeding 9% in single-junction cells[4-7] and reaching a milestone value of 10% in tandem cells,[8,9] the improvement of PCE remains a formidable challenge.

As has been demonstrated by studies on PSCs, the development of semiconducting polymers with alternating electron-rich (donor; D) and electron-poor (acceptor; A) building units, i.e. D–A polymers, is a key to improving PCE.[10-13] D–A polymers afford absorption bands in the long-wavelength region, i.e., a small bandgap, due to orbital mixing between the D and A units, which produces a large short-circuit current (J_{SC}) in PSCs. In line with this design strategy numerous D–A semiconducting polymers have been synthesized. Examples of pioneering works include a cyclopentadithiophene–benzothiadiazole polymer (PCPDTBT),[14,15] a carbazole–benzothiadiazole polymer (PCDTBT),[16,17] or a series of benzodithiophene–thienothiophene polymers (PTBs).[18-20]

We have previously reported that a new D–A polymer with quaterthiophene and naphtho[1,2-*c*:5,6-*c*′]bis[1,2,5]thiadiazole (NTz)[21,22] as the D and A units, respectively (PNTz4T, Figure 1). This polymer is promising as it shows a high PCE of 6.3% in single-junction PSCs that use [6,6]-phenyl-C61-butyric acid methyl ester ($PC_{61}BM$) as the n-type material thanks to its long-wavelength absorption in the range of 300–800 nm and a relatively large ionization potential of 5.15 eV.[23] Another striking feature of PNTz4T is that it forms a crystalline structure with a lamellar motif in which the polymer backbones are π-stacked with a distance of ca. 3.5 Å in the thin

film. This π–π stacking distance is short compared with that of typical high-performance D–A polymers used in PSCs,[24,25] owing to the strong intermolecular interactions most likely originating in the NTz-based backbone structure. In addition, PNTz4T forms a "face-on" orientation in the polymer/$PC_{61}BM$ blend film, which is favourable for PSCs, whereas it forms an "edge-on" orientation in the polymer neat film suitable for transistors, in which high field-effect hole mobilities of up to 0.5 $cm^2\ V^{-1}\ s^{-1}$ was observed. The high crystallinity and the favourable backbone orientation well rationalize the high photovoltaic performance of PNTz4T. Here, we demonstrate that through further studies of PNTz4T, PCEs of 10% can be achieved in a single-junction PSC with the inverted architecture and the active layer thickness of ca. 300 nm, which is much larger than that of typical PSCs. Importantly, we found that the face-on orientation is more abundant and that the distribution of the edge-on/face-on orientation through the film thickness is more favourable in the inverted cell than in the conventional cell, which should be key factors for understanding the origin of the high performance in PNTz4T cells.

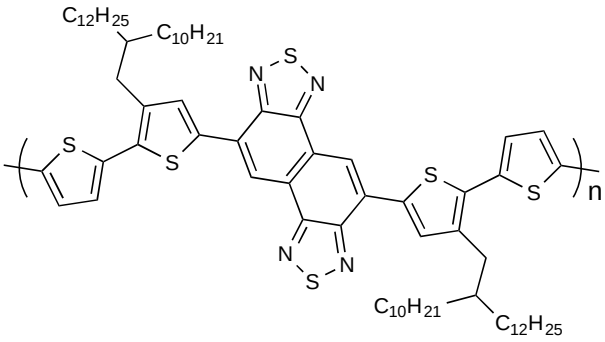

Figure 1. Chemical structure of PNTz4T, a quaterthiophene–naphthobisthiadiazole (NTz) copolymer.

Solar cell fabrications and performance

Solar cells with conventional and inverted architectures were fabricated. The cells were composed of indium tin oxide (ITO)/ poly(3,4-ethylenedioxythiophene):polystyrene sulfonate (PEDOT:PSS)/PNTz4T:$PC_{61}BM$ or [6,6]-phenyl-C71-butyric acid methyl ester ($PC_{71}BM$)/LiF/Al and ITO/ZnO/PNTz4T:$PC_{61}BM$ or $PC_{71}BM/MoO_x$/Ag, respectively. The PNTz4T to PCBM weight ratio was 1:2 in all cases. The active layer was fabricated by spin-coating the polymer/PCBM blend solution in *o*-dichlorobenzene (DCB). Note that no solvent additives such as 1,8-diiodooctane (DIO), which are often used in order to promote the phase separation, were used in this system.

In a conventional cell that used $PC_{61}BM$, PCE of 6.55%, with J_{SC} of 12.1 mA cm^{-2}, the open-circuit voltage (V_{OC}) of 0.746 V, and the fill factor (FF) of 72.7% were obtained when the active layer thickness was 150 nm (Figure S1, Table S1). The observed FF is fairly high considering that the active layer is 1.5–2 times thicker than that of typical PSCs (70–100 nm). Then, we fabricated cells with even thicker active layers (Figure S1, Table S1). Similarly to previous studies that used thicker active layers,[26-30] J_{SC} increased with the increase of the thickness. V_{OC} slightly decreased with the increase of the thickness, but the change was relatively small. Although FF showed gradual decrease, it remained moderately high with the value of 66.7% at 300 nm. As a result, the overall PCE reached 8.70% with J_{SC} of 17.7 mA cm^{-2} and V_{OC} of 0.738 V at 300 nm (Figure 2a, Table 1). The external quantum efficiency (EQE) was generally high; it was around 70% in the polymer absorption ranges of 300 to 500 nm and 600 to 800 nm (Figure 2b). In the conventional cell using $PC_{71}BM$, a large J_{SC} was obtained compared with the cell using $PC_{61}BM$ (Figure 2a), which is due to the increased absorption and thus the high EQE in the range of 500–600 nm (Figure 2b), as commonly observed for PSCs. The $PC_{71}BM$ cells exhibited dependence of the photovoltaic parameters on the active layer thickness (Figure S2, Table S2) similarly to the $PC_{61}BM$

cell, and gave the highest PCE of 8.92% with the 290 nm thick active layer (Table 1).

Interestingly, the inverted cells demonstrated high photovoltaic performances, in particular J_{SC} and FF, as compared to the conventional cells, as seen in other polymer systems (Figures 2a and 2b, Table 1).[4,31,32] The inverted cells also showed the thickness dependence of the photovoltaic performance (Figures S3 and S4 and Tables S3 and S4). Notably, PCE reached 10.1% (J_{SC} = 19.4 mA cm^{-2}, V_{OC} = 0.708 V, FF = 73.4%) with the average of 9.77% for the inverted $PC_{71}BM$ cell that had the active layer thickness of around 290 nm, which is one of the highest PCEs observed for a single-junction cell. It is interesting to note that PCEs close to 10% were also observed for the inverted $PC_{61}BM$ cell that had the thickness of 280 nm (PCE = 9.80% (average 9.55%), J_{SC} = 18.2 mA cm^{-2}, V_{OC} = 0.729 V, FF = 73.9%).

To investigate the reason for higher FF in the inverted cell than in the conventional cells, we conducted a qualitative study of the difference in charge recombination between the two device architectures by plotting J_{SC} and FF as a function of light intensity (Figures 2c and 2d).[33] It is clear that for both conventional and inverted $PC_{61}BM$ and $PC_{71}BM$ cells, J_{SC} increases linearly as the light intensity increases, wherein the number of free carriers increases. As regards FF, its decrease with increasing light intensity was milder in the inverted cells than in the conventional cells. The difference in the decrease of FF implies that bimolecular recombination is reduced in the inverted cell compared with the conventional cell, which may be one of the reasons for the higher FF in the inverted cell of this system.

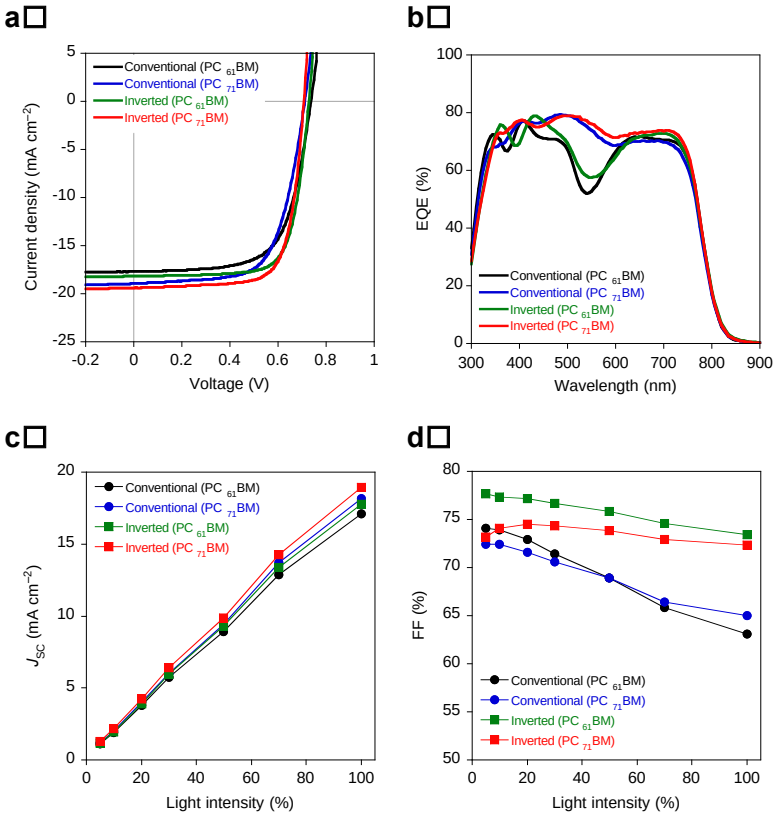

Figure 2. Photovoltaic characteristics of PNTz4T-based cells with the conventional (ITO/PEDOT:PSS/PNTz4T:$PC_{61}BM$ or $PC_{71}BM$/LiF/Al) and the inverted (ITO/ZnO/PNTz4T:$PC_{61}BM$ or $PC_{71}BM$/MoO_x/Ag) architecture. (a) Current density–voltage (*J*–*V*) curves and (b) external quantum efficiency spectra of the best cells. (c) J_{SC} and (d) FF as a function of light intensity.

Table 1. Photovoltaic parameters of the best PNTz4T solar cells.

Cell structure	PCBM	thickness (nm)	J_{SC} (mA cm^{-2})	V_{OC} (V)	FF (%)	PCE_{max} [PCE_{ave}] (%)
conventional	$PC_{61}BM$	300	17.7	0.738	66.7	8.70 [8.46]
	$PC_{71}BM$	290	18.9	0.712	66.2	8.92 [8.65]
inverted	$PC_{61}BM$	280	18.2	0.729	73.9	9.80 [9.55]
	$PC_{71}BM$	290	19.4	0.708	73.4	10.1 [9.77]

thickness: active layer thickness, PCE_{max}: maximum power conversion efficiency, PCE_{ave}: average power conversion efficiency

Charge transport property

Charge carrier mobilities of the blend films in the direction vertical to the substrate plane were evaluated by using hole-only (ITO/PEDOT:PSS/active layer/MoO_x/Ag) and electron-only (ITO/ZnO/active layer/LiF/Al) devices (Figures S8 and S9). The polymer neat film was also evaluated in the hole-only device (Figure S8). Both hole (μ_h) and electron (μ_e) mobilities were obtained by using the space-charge limited current model. Whereas μ_h for the polymer neat film was 7.2×10^{-4} cm^2 V^{-1} s^{-1}, those for the blend films with $PC_{61}BM$ and $PC_{71}BM$ were 2.1×10^{-3} cm^2 V^{-1} s^{-1} and 3.4×10^{-3} cm^2 V^{-1} s^{-1}, respectively. Higher μ_h for the blend film than for the polymer neat film is likely due to the more favourable backbone orientation for the vertical charge transport in the blends.[23] The μ_h values for the blends are fairly high for the semiconducting polymers,[19] and most likely originate in the combination of the highly crystalline structure along with the short π–π stacking distance (3.5 Å), and the favourable face-on orientation. It should be noted that μ_e was also of the order of 10^{-3} cm^2 V^{-1} s^{-1} (2.3×10^{-3} cm^2 V^{-1} s^{-1} for the blend film with $PC_{61}BM$, and 1.1×10^{-3} cm^2 V^{-1} s^{-1} for that with $PC_{71}BM$). These results are indicative of the well-balanced hole and electron transport in the PNTz4T/PCBM blend films, and rationalize the high photovoltaic performance for the PNTz4T cells.

Grazing incidence wide-angle X-ray diffraction studies

Polymer microstructures in the blend films were studied by grazing incidence wide-angle X-ray diffraction (GIWAXD) measurements. Figures 3a and 3b display the two-dimensional (2D) GIWAXD images of PNTz4T/$PC_{61}BM$ blend films spun on ITO/PEDOT:PSS and ITO/ZnO substrates (film thickness: ca. 250 nm). In both cases, a diffraction corresponding to the π–π stacking appeared only along the q_z axis (out-of-plane direction), suggesting that there is a large population of polymer crystallites with the face-on orientation.[34] Nevertheless, diffractions corresponding to the lamellar structure appeared along both the q_z and q_{xy} (in-plane direction) axes, indicating that edge-on and face-on crystallites co-exist in the film. These results indicate that the polymer easily forms a crystalline structure in the blend films by spin coating from DCB solution on both the substrates. The fact that PNTz4T/$PC_{71}BM$ blend films also showed similar textures to the PNTz4T/$PC_{61}BM$ blend films (Figure S11) suggests that there is no significant difference in polymer crystallinity and orientation between the $PC_{61}BM$ and $PC_{71}BM$ blend films.

To gain a deeper insight into the orientation, we performed a pole figure analysis of the blend films.[35,36] Figure 3c shows the pole figures extracted from the lamellar diffraction, (100), of PNTz4T in the 2D GIWAXD patterns for the PNTz4T/$PC_{61}BM$ blend films on the ITO/PEDOT:PSS and ITO/ZnO substrates with the ca. 250 nm thickness as shown in Figures 3a and 3b (see also the insets for a close-up of the lamellar diffraction). We defined that the areas integrated with the polar angle (χ) ranges of 0–45° and 135–180° (A_z) and 55–125° (A_{xy}) as those corresponding to the fractions of the edge-on and face-on crystallites, respectively. It is interesting to note that the ratio of A_{xy} to A_z (A_{xy}/A_z) for the blend film on the ITO/ZnO substrate was 0.79, which was higher than that for the blend film on the ITO/PEDOT:PSS substrate, namely, 0.64. This means that the population of the face-on crystallite is larger in the inverted cells than in the

conventional cells. This could be attributed to the difference in wettability of the solution on the substrate surfaces. It has been reported that substrate surfaces with lower wettability induce higher tendency of edge-on orientation to semiconducting polymers in the thin film by spin coating the polymer solution.[37] We therefore measured the contact angle of DCB, the solvent used for the spin-coating, on the PEDOT:PSS and ZnO surfaces (both coated on the ITO glass substrate), and those average values were 18.5° and 6.1°, respectively (Figure S17). This suggests that the PEDOT:PSS surface has low wettability relative to the ZnO surface, which may explain the larger population of edge-on orientation on the PEDOT:PSS surface (larger population of face-on orientation on the ZnO surface).

We also carried out the pole figure analysis of the PNTz4T/$PC_{61}BM$ blend films on the ITO/PEDOT:PSS and ITO/ZnO substrates with different thicknesses, from ca. 50 nm to 400 nm (Figures S12 and S14), and plotted A_{xy}/A_z as a function of film thickness (Figure 3d). For all the thicknesses, A_{xy}/A_z was larger in the ITO/ZnO substrate than in the ITO/PEDOT:PSS substrate. Notably, A_{xy}/A_z gradually increased with the increase of the film thickness in both cases, i.e., the population of the face-on crystallites increased with the film thickness. This suggests that the face-on to edge-on ratio is not distributed evenly along the film thickness. One can assume that the orientation in the interfacial layers at the bottom (PEDOT:PSS or ZnO) and air, as well as the thickness of the interfacial layer, is independent of the total film thickness. Thus, this increase of the face-on crystallite population mainly occurs at the bulk, which arises from the increase of the bulk volume in thicker films. This means that the edge-on crystallites are abundant either at the film/bottom or film/air interface. It has been reported previously that, in the regioregular poly(3-hexylthiophene) films, the edge-on crystallites exist at the film/bottom layer interface and the face-on crystallites exist in the bulk and the film/air interface.[38,39] Thus, in the case of PNTz4T,

a class of polythiophene-based polymer, it is natural to consider that the edge-on crystallites are abundant at the film/bottom layer interface, and the face-on crystallites are abundant in the bulk through the film/air interface, regardless of the substrate. The PNTz4T/PC_{71}BM blend film provided the similar results to the PNTz4T/PC_{61}BM blend film (Figures S13, S15 and S16).

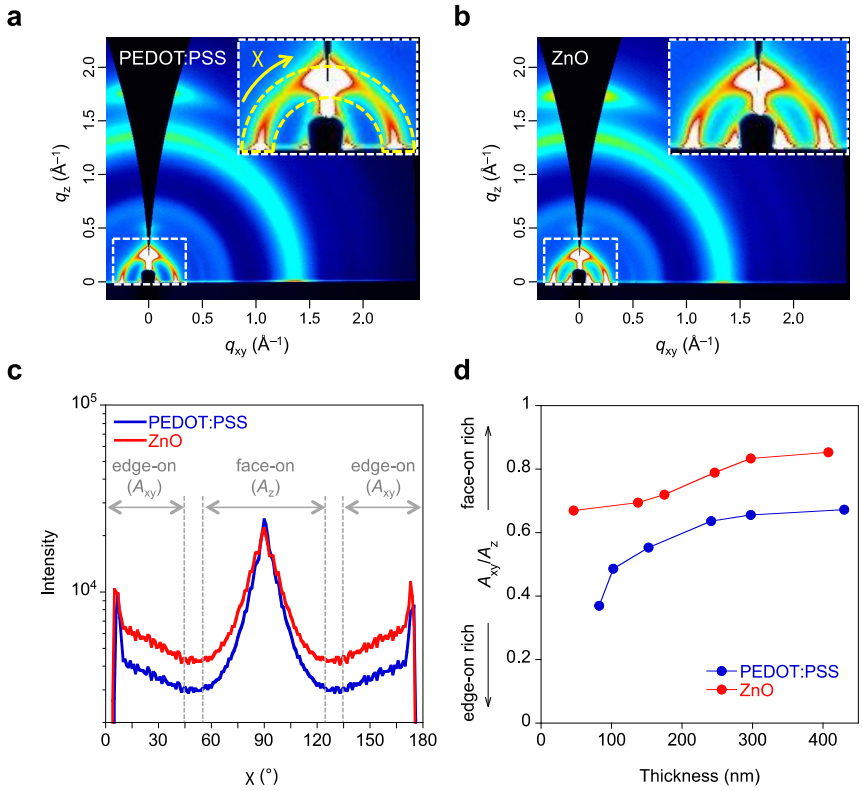

Figure 3. GIWAXD data for PNTz4T/$PC_{61}BM$ blend films. (a) 2D GIWAXD image of the blend film on the ITO/PEDOT:PSS substrate (thickness: 241 nm). (b) 2D GIWAXD image of the blend film on the ITO/ZnO substrate (thickness: 246 nm). Insets show a close-up of the lamellar, (100), diffraction region. (c) Pole figures extracted from the lamellar diffraction for the blend films on both ITO/PEDOT:PSS and ITO/ZnO substrates. Definition of the polar angle (χ) range corresponding to the edge-on (A_z) and face-on (A_{xy}) crystallites are also shown. (d) Dependence of A_{xy}/A_z on the film thickness. A_{xy}/A_z is a figure that represents the ratio of the face-on to edge-on orientation.

Discussion

We discuss herein the rationale for the markedly high performance of PNTz4T-based cells fabricated using the thicker active layer with the inverted architecture. We assume that the high FF and thus the high efficiency observed even with thicker films is attributed to the quite high vertical hole transport of the polymer (μ_h = 2–3 × 10^{-3} cm^2 V^{-1} s^{-1}).[20,28,29] This apparently originates in the highly crystalline structure with the short π–π stacking distance, and the well-balanced hole and electron transport.

It has been reported by several groups that the vertical phase gradation of the polymer and PCBM, which is characterized by polymer enrichment at the film/top interlayer (film/air) interface and PCBM enrichment at the film/bottom interlayer interface, is responsible for the increased performance in the inverted cells.[31,32] In contrast, the energy-dispersive X-ray spectroscopy (EDS) of the cross section revealed that in all the PNTz4T cells the sulfur content was weakly increased from the film/top interface to the film/bottom interface (Figure S19). This suggests that the polymer is weakly but gradually enriched toward the film/bottom layer interface. This "reverse" vertical polymer concentration gradation should be disadvantageous for the inverted architecture.

Instead, we found that PNTz4T shows a higher tendency to form the favourable face-on orientation on the ZnO surface than on the PEDOT:PSS surface, which correspond to the inverted and conventional cells, respectively. It is also important to mention that we observed unevenly distributed polymer orientations through the film thickness, as revealed by the in-depth GIWAXD studies. The population of the face-on crystallites is larger in the bulk through the film/top interlayer interface, i.e., the film/LiF (conventional cell) or MoO_x (inverted cell) top interfaces, and the population of the edge-on crystallites is larger at the film/bottom interlayer interface, i.e., the film/PEDOT:PSS (conventional cells) or film/ZnO (inverted cells) interfaces, as illustrated in

Figure 4. Therefore, in the conventional cells, where the generated holes flow toward the bottom PEDOT:PSS layer through the edge-on-rich region, this distribution of the polymer orientation should be detrimental to the vertical hole transport, resulting in the inefficient hole collection. In contrast, in the inverted cells, where the holes flow toward the top MoO_x layer through the face-on-rich region, this polymer orientation distribution would facilitate the vertical hole transport, leading to the efficient hole collection. This model is in good agreement with the high J_{SC} and FF, as well as the reduced charge recombination, in the inverted cell compared with the conventional cell.

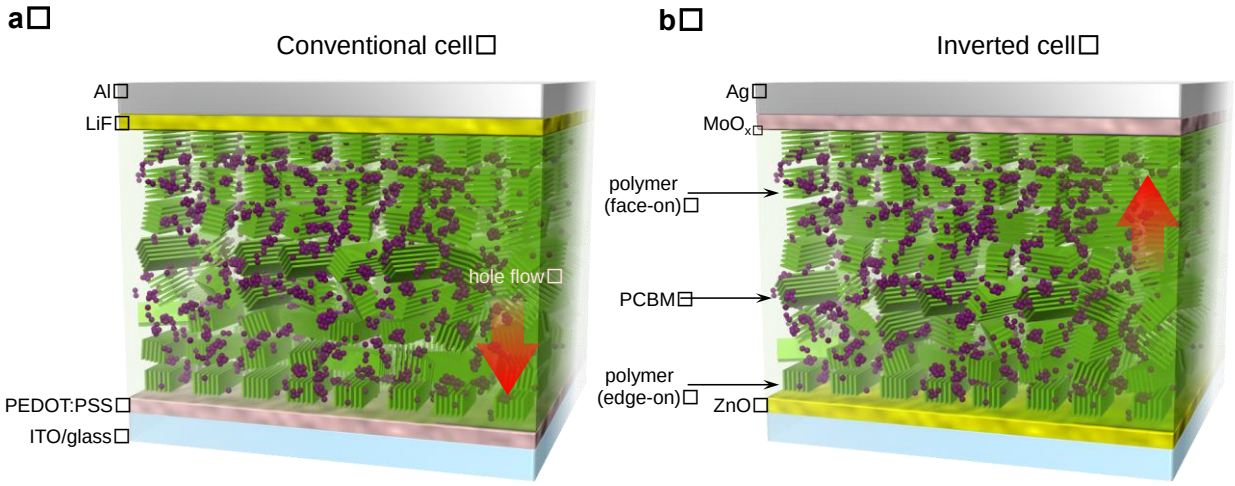

Figure 4. Schematic illustrations of PNTz4T/$PC_{61}BM$ blend films in the solar cells. (a) Conventional cell with PEDOT:PSS as the bottom and LiF as the top interlayer. (b) Inverted cell with ZnO as the bottom and MoO_x as the top interlayer. The population of face-on crystallite is larger in the inverted cell than in the conventional cell. In both cases, the population of edge-on crystallites is large at the bottom interface and the population of face-on crystallites is large in the bulk through the top interface. Note that the amount of PCBM is markedly reduced as compared with the real cells and the distribution of the orientation is exaggerated in order to better visualize the polymer orientation.

Conclusions

We have demonstrated PCE reaching 10% in single-junction PSCs with the inverted architecture, using PNTz4T as the p-type material and $PC_{71}BM$ as the n-type material. Notably, these results has been achieved by using the thick active layer measuring around 300 nm which is far thicker than the typical thickness for PSCs and is beneficial for the practical use.[26,28] The high efficiency is most likely attributed to the highly ordered polymer structure in the active layer, in which the highly crystalline structure with the short π–π stacking distance and the favourable face-on orientation are achieved. Importantly, we found that the polymer crystallites with the face-on orientation are present in greater abundance on the ZnO surface than on the PEDOT:PSS surface, and that the face-on orientation is enriched in the bulk and at the top contact and the edge-on orientation is enriched at the bottom contact. These unique characteristics in the backbone orientation would facilitate charge transport and reduce charge recombination particularly in the inverted architecture, resulting in the higher J_{SC} and FF. These results are evidence of the great promise of PSCs, and indicate that further higher PCEs should be realized by careful molecular design using the NTz moiety.

Methods

Materials. PNTz4T samples were synthesized according to the reported procedure.[23] The molecular weights (M_n) of the samples were 50–60 kDa and the polydispersity index (PDI) was around 2.5. $PC_{61}BM$ and $PC_{71}BM$ were purchased from Frontier Carbon Corporation, Solenne BV, and Luminescent Technology Corporation. $PC_{61}BM$s and $PC_{71}BM$s from different suppliers gave similar results. PEDOT:PSS (Clevios P VP Al 4083) was purchased from Heraeus. The patterned ITO-coated glass substrates were purchased from Atsugi Micro, Co. Ltd.

Thin film characterization. GIWAXD experiments were conducted at the SPring-8 on beamline BL46XU. The sample was irradiated with an X-ray energy of 12.39 keV (λ = 1 Å) at a fixed incident angle on the order of 0.12° through a Huber diffractometer. The GIWAXD patterns were recorded with a two-dimensional image detector (Pilatus 300K). Energy-dispersive X-ray spectroscopy (EDS) was performed with an atomic resolution analytical electron microscope (JEOL, Ltd., JEM-ARM200F).

Solar cells fabrication and characterization. ITO substrates were pre-cleaned sequentially by sonicating in a detergent bath, de-ionized water, acetone, and isopropanol at rt, and in a boiled isopropanol bath, each for 10 min. Then, the substrates were subjected to UV/ozone treatment at rt for 20 min. For conventional cells, the pre-cleaned ITO substrates were coated with PEDOT:PSS by spin coating (5000 rpm for 30 sec, thickness: ~30 nm), and then baked at 120 °C for 15 min in air. The active layer was deposited in a glove box by spin coating hot (100 ºC) DCB solution containing PNTz4T and $PC_{61}BM$ or $PC_{71}BM$ with the weight ratio of 1:2 at 600 rpm for 20 sec. The active layer thickness was controlled by changing the concentration of the solution, e.g., an 8 g/L solution

(based on the polymer concentration) typically gave an active layer of 250–300 nm thickness. The thin films were transferred into a vacuum evaporator connected to the glove box, and LiF (0.8 nm) and Al (100 nm) were deposited sequentially through a shadow mask under ~10^{-5} Pa, where the active area of the cells was 0.16 cm^2. For the inverted cells, the pre-cleaned ITO substrates masked at the electrical contacts were coated with ZnO precursor by spin coating (3000 rpm for 30 sec) a precursor solution prepared by dissolving zinc acetate dehydrate (0.5 g) and ethanolamine (0.14 mL) in 5 mL of 2-methoxyethanol. They were then baked in air at 200 ºC for 30 min, then rinsed with acetone and isopropanol, and dried in a glove box. The active layer was deposited as described above. MoOx (7.5 nm) and Ag (100 nm) were deposited sequentially by thermal evaporation under ~10^{-5} Pa.

J–V characteristics of the cells were measured with a Keithley 2400 source measure unit in nitrogen atmosphere under 1 Sun (AM1.5G) conditions using a solar simulator (SAN-EI Electric, XES-40S1, 1000 W m^{-2}). More than 20 cells have been analysed to provide average efficiencies for the optimized cells. The cell data with the use of a photomask (0.1225 cm^2) were consistent with those without the photomask (Figure S5, Table S5). No hysteresis was observed in the *J–V* curves (Figure S6). PNTz4T/PC_{71}BM cells were also characterized at Japan Electrical Safety & Environment Technology Laboratories (JET) (Figure S7). The light intensity for the *J–V* measurements was calibrated with a reference PV cell (Konica Minolta AK-100 certified by the National Institute of Advanced Industrial Science and Technology, Japan). EQE spectra were measured with a Spectral Response Measuring System (Soma Optics, Ltd., S-9241). The thickness of the active layer was measured with an AlphaStep® D-100 surface profiler (KLA Tencor).

Hole-only and electron-only devices fabrication and measurement.[40] For hole-only devices, the

pre-cleaned ITO substrates were coated with PEDOT:PSS by spin-coating (5000 rpm for 30 sec, thickness: ~30 nm). Then, the PNTz4T film or the PNTz4T/$PC_{61}BM$ or $PC_{71}BM$ (1:2 weight ratio) blend film was spin coated from a hot (100 °C) DCB solution (8 g/L based on the polymer concentration) at 600 rpm for 20 sec. The thin films were transferred into a vacuum evaporator connected to the glove box, and MoO_x (7.5 nm) and Ag (100 nm) were deposited sequentially through a shadow mask. For electron-only devices, the pre-cleaned ITO substrates were coated with ZnO, and then with the PNTz4T/$PC_{61}BM$ or $PC_{71}BM$ (1:2 weight ratio) blend film as described above. LiF (2 nm) and Al (100 nm) were deposited sequentially. *J*–*V* characteristics were measured in the range of 0−7 V using a Keithley 2400 source measure unit under nitrogen in the dark, and the mobility was calculated by fitting the *J*–*V* curves to a space charge limited current model described by

$$J = (8/9)\, \varepsilon_r\, \varepsilon_0\, \mu\, (V^2/L^3)$$

where ε_r is the dielectric constant of the polymer, ε_0 is the permittivity of free space, μ is the mobility, $V = V_{appl} - V_{bi}$, where V_{appl} is the applied voltage to the device and V_{bi} is the built-in voltage due to the difference in work function of the two electrodes, which is determined to be 0.1 for the hole-only device and 0.1 for the electron-only device, and L is the polymer thickness. The dielectric constant ε_r is assumed to be 3, which is a typical value for semiconducting polymers.

References

1 Yu, G., Gao, J., Hummelen, J. C., Wudl, F. & Heeger, A. J. Polymer Photovoltaic Cells: Enhanced Efficiencies via a Network of Internal Donor-Acceptor Heterojunctions. *Science* **270**, 1789-1791 (1995).

2 Günes, S., Neugebauer, H. & Sariciftci, N. S. Conjugated Polymer-Based Organic Solar Cells. *Chem. Rev.* **107**, 1324-1338 (2007).

3 Brabec, C., Dyakonov, V. & Scherf, U. *Organic Photovoltaics: Materials, Device Physics, and Manufacturing Technologies*. (Wiley-VCH, 2008).

4 He, Z., Zhong, C., Su, S., Xu, M., Wu, H. & Cao, Y. Enhanced power-conversion efficiency in polymer solar cells using an inverted device structure. *Nat. Photon.* **6**, 591-595 (2012).

5 Ye, L., Zhang, S., Zhao, W., Yao, H. & Hou, J. Highly Efficient 2D-Conjugated Benzodithiophene-Based Photovoltaic Polymer with Linear Alkylthio Side Chain. *Chem. Mater.* (2014).

6 Liao, S.-H., Jhuo, H.-J., Yeh, P.-N., Cheng, Y.-S., Li, Y.-L., Lee, Y.-H., Sharma, S. & Chen, S.-A. Single Junction Inverted Polymer Solar Cell Reaching Power Conversion Efficiency 10.31% by Employing Dual-Doped Zinc Oxide Nano-Film as Cathode Interlayer. *Sci. Rep.* **4**, 6813 (2014).

7 Liu, Y., Zhao, J., Li, Z., Mu, C., Ma, W., Hu, H., Jiang, K., Lin, H., Ade, H. & Yan, H. Aggregation and morphology control enables multiple cases of high-efficiency polymer solar cells. *Nat Commun* **5**, 5293 (2014).

8 You, J., Dou, L., Yoshimura, K., Kato, T., Ohya, K., Moriarty, T., Emery, K., Chen, C.-C., Gao, J., Li, G. & Yang, Y. A polymer tandem solar cell with 10.6% power conversion efficiency. *Nat. Commun.* **4**, 1446 (2013).

9 You, J., Chen, C.-C., Hong, Z., Yoshimura, K., Ohya, K., Xu, R., Ye, S., Gao, J., Li, G. & Yang, Y. 10.2% Power Conversion Efficiency Polymer Tandem Solar Cells Consisting of Two Identical Sub-Cells. *Adv. Mater.* **25**, 3973-3978 (2013).

10 Scharber, M. C., Mühlbacher, D., Koppe, M., Denk, P., Waldauf, C., Heeger, A. J. & Brabec, C. J. Design Rules for Donors in Bulk-Heterojunction Solar Cells—Towards 10 % Energy-Conversion Efficiency. *Adv. Mater.* **18**, 789-794 (2006).

11 Facchetti, A. π -Conjugated Polymers for Organic Electronics and Photovoltaic Cell Applications. *Chem. Mater.* **23**, 733-758 (2011).

12 Boudreault, P.-L. T., Najari, A. & Leclerc, M. Processable Low-Bandgap Polymers for Photovoltaic Applications. *Chem. Mater.* **23**, 456-469 (2011).

13 Beaujuge, P. M. & Fréchet, J. M. J. Molecular design and ordering effects in π -functional materials for transistor and solar cell applications. *J. Am. Chem. Soc.* **133**, 20009-20029 (2011).

14 Mühlbacher, D., Scharber, M., Morana, M., Zhu, Z., Waller, D., Gaudiana, R. & Brabec, C. High Photovoltaic Performance of a Low-Bandgap Polymer. *Adv. Mater.* **18**, 2884-2889 (2006).

15 Peet, J., Kim, J. Y., Coates, N. E., Ma, W. L., Moses, D., Heeger, A. J. & Bazan, G. C. Efficiency enhancement in low-bandgap polymer solar cells by processing with alkane dithiols. *Nature Mater.* **6**, 497-500 (2007).

16 Blouin, N., Michaud, A., Gendron, D., Wakim, S., Blair, E., Neagu-Plesu, R., Belletête, M., Durocher, G., Tao, Y. & Leclerc, M. Toward a rational design of poly (2, 7-carbazole) derivatives for solar cells. *J. Am. Chem. Soc.* **130**, 732-742 (2008).

17 Park, S. H., Roy, A., Beaupre, S., Cho, S., Coates, N., Moon, J. S., Moses, D., Leclerc, M.,

Lee, K. & Heeger, A. J. Bulk heterojunction solar cells with internal quantum efficiency approaching 100%. *Nat. Photon.* **3**, 297-302 (2009).

18 Liang, Y., Wu, Y., Feng, D., Tsai, S.-T., Son, H.-J., Li, G. & Yu, L. Development of New Semiconducting Polymers for High Performance Solar Cells. *J. Am. Chem. Soc.* **131**, 56-57 (2009).

19 Liang, Y., Feng, D., Wu, Y., Tsai, S. T., Li, G., Ray, C. & Yu, L. Highly efficient solar cell polymers developed via fine-tuning of structural and electronic properties. *J. Am. Chem. Soc.* **131**, 7792-7799 (2009).

20 Liang, Y., Xu, Z., Xia, J., Tsai, S.-T., Wu, Y., Li, G., Ray, C. & Yu, L. For the Bright Future-Bulk Heterojunction Polymer Solar Cells with Power Conversion Efficiency of 7.4%. *Adv. Mater.* **22**, E135-E138 (2010).

21 Mataka, S., Takahashi, K., Ikezaki, Y., Hatta, T., Tori-i, A. & Tashiro, M. Sulfur nitride in organic chemsitry. XIV, Selective formation of benzo-and benzobis [1, 2, 5] thiadiazole skeleton in the reaction of tetrasulfur tetranitride with naphthalenols and related compounds. *Bull. Chem. Soc. Jpn.* **64**, 68-73 (1991).

22 Wang, M., Hu, X., Liu, P., Li, W., Gong, X., Huang, F. & Cao, Y. A Donor-Acceptor Conjugated Polymer Based on Naphtho [1, 2-c: 5, 6-c] bis [1, 2, 5] thiadiazole for High Performance Polymer Solar cells. *J. Am. Chem. Soc.* **133**, 9638–9641 (2011).

23 Osaka, I., Shimawaki, M., Mori, H., Doi, I., Miyazaki, E., Koganezawa, T. & Takimiya, K. Synthesis, Characterization, and Transistor and Solar Cell Applications of a Naphthobisthiadiazole-Based Semiconducting Polymer. *J. Am. Chem. Soc.* **134**, 3498-3507 (2012).

24 Szarko, J. M., Guo, J., Liang, Y., Lee, B., Rolczynski, B. S., Strzalka, J., Xu, T., Loser, S.,

Marks, T. J., Yu, L. & Chen, L. X. When Function Follows Form: Effects of Donor Copolymer Side Chains on Film Morphology and BHJ Solar Cell Performance. *Adv. Mater.* **22**, 5468-5472 (2010).

25 Guo, X., Zhou, N., Lou, S. J., Hennek, J. W., Ponce Ortiz, R., Butler, M. R., Boudreault, P.-L. T., Strzalka, J., Morin, P.-O., Leclerc, M., López Navarrete, J. T., Ratner, M. A., Chen, L. X., Chang, R. P. H., Facchetti, A. & Marks, T. J. Bithiopheneimide–Dithienosilole/Dithienogermole Copolymers for Efficient Solar Cells: Information from Structure–Property–Device Performance Correlations and Comparison to Thieno[3,4-c]pyrrole-4,6-dione Analogues. *J. Am. Chem. Soc.* **134**, 18427-18439 (2012).

26 Peet, J., Wen, L., Byrne, P., Rodman, S., Forberich, K., Shao, Y., Drolet, N., Gaudiana, R., Dennler, G. & Waller, D. Bulk heterojunction solar cells with thick active layers and high fill factors enabled by a bithiophene-co-thiazolothiazole push-pull copolymer. *Appl. Phys. Lett.* **98**, 043301 (2011).

27 Price, S. C., Stuart, A. C., Yang, L., Zhou, H. & You, W. Fluorine Substituted Conjugated Polymer of Medium Band Gap Yields 7% Efficiency in Polymer− Fullerene Solar Cells. *J. Am. Chem. Soc.* **133**, 4625-4631 (2011).

28 Li, W., Hendriks, K. H., Roelofs, W. S. C., Kim, Y., Wienk, M. M. & Janssen, R. A. J. Efficient Small Bandgap Polymer Solar Cells with High Fill Factors for 300 nm Thick Films. *Adv. Mater.*, 3182–3186 (2013).

29 Osaka, I., Kakara, T., Takemura, N., Koganezawa, T. & Takimiya, K. Naphthodithiophene–Naphthobisthiadiazole Copolymers for Solar Cells: Alkylation Drives the Polymer Backbone Flat and Promotes Efficiency. *J. Am. Chem. Soc.* **135**, 8834-8837 (2013).

30 Osaka, I., Saito, M., Koganezawa, T. & Takimiya, K. Thiophene–Thiazolothiazole Copolymers: Significant Impact of Side Chain Composition on Backbone Orientation and Solar Cell Performances. *Adv. Mater.* **26**, 331-338 (2014).

31 Xu, Z., Chen, L.-M., Yang, G., Huang, C.-H., Hou, J., Wu, Y., Li, G., Hsu, C.-S. & Yang, Y. Vertical Phase Separation in Poly(3-hexylthiophene): Fullerene Derivative Blends and its Advantage for Inverted Structure Solar Cells. *Adv. Funct. Mater.* **19**, 1227-1234 (2009).

32 Guo, X., Zhou, N., Lou, S. J., Smith, J., Tice, D. B., Hennek, J. W., Ortiz, R. P., Navarrete, J. T. L., Li, S., Strzalka, J., Chen, L. X., Chang, R. P. H., Facchetti, A. & Marks, T. J. Polymer solar cells with enhanced fill factors. *Nat. Photon.* **7**, 825-833 (2013).

33 Stuart, A. C., Tumbleston, J. R., Zhou, H., Li, W., Liu, S., Ade, H. & You, W. Fluorine Substituents Reduce Charge Recombination and Drive Structure and Morphology Development in Polymer Solar Cells. *J. Am. Chem. Soc.* **135**, 1806-1815 (2013).

34 Sirringhaus, H., Brown, P., Friend, R. & Nielsen, M. Two-dimensional charge transport in self-organized, high-mobility conjugated polymers. *Nature* **401**, 685-688 (1999).

35 Baker, J. L., Jimison, L. H., Mannsfeld, S., Volkman, S., Yin, S., Subramanian, V., Salleo, A., Alivisatos, A. P. & Toney, M. F. Quantification of Thin Film Crystallographic Orientation Using X-ray Diffraction with an Area Detector. *Langmuir* **26**, 9146-9151 (2010).

36 Rivnay, J., Mannsfeld, S. C. B., Miller, C. E., Salleo, A. & Toney, M. F. Quantitative Determination of Organic Semiconductor Microstructure from the Molecular to Device Scale. *Chem. Rev.* **112**, 5488-5519 (2012).

37 Umeda, T., Kumaki, D. & Tokito, S. Surface-energy-dependent field-effect mobilities up to 1 cm2/V s for polymer thin-film transistor. *J. Appl. Phys.* **105**, 024516 (2009).

38 Kline, R., McGehee, M. & Toney, M. Highly oriented crystals at the buried interface in

polythiophene thin film transistors. *Nature Mater.* **5**, 222-228 (2006).

39 Duong, D. T., Toney, M. F. & Salleo, A. Role of confinement and aggregation in charge transport in semicrystalline polythiophene thin films. *Phys. Rev. B* **86**, 205205 (2012).

40 Shrotriya, V., Yao, Y., Li, G. & Yang, Y. Effect of self-organization in polymer/fullerene bulk heterojunctions on solar cell performance. *Appl. Phys. Lett.* **89**, 063505 (2006).

Acknowledgements

This research was supported by Grant-in-Aid for Scientific Research from The Ministry of Education, Culture, Sports, Science and Technology (Nos. 24685030 and 23245041), and by Precursory Research for Embryonic Science and Technology from Japan Science and Technology Agency. 2D GIWAXD experiments were performed at SPring-8 with the approval of the Japan Synchrotron Radiation Research Institute (JASRI) (Proposal No. 2014A1530). The authors thank Dr. K. Tajima of CEMS, RIKEN for helpful discussion on the fabrication of inverted cells and for the contact angle measurement, and Dr. K. Higashimine of the Center for Nano Materials and Technology, JAIST for the EDS measurement. The authors thank Dr. Y. Hishikawa of National Institute of Advanced Industrial Science and Technology (AIST) and Dr. H. Tobita of Japan Electrical Safety & Environment Technology Laboratories (JET) for the technical discussion of *J–V* measurement. The authors also thank Dr. Y. Hishikawa and A. Sasaki for the measurement of active area of the cell.

Author contributions

K.K. prepared the polymer sample. V.V. and I.O. conceived and designed the solar cell experiments. V.V. and K.K. fabricated the conventional cells, and K.K. and T.Kakara fabricated the inverted cells. I.O. and T.Koganezawa conceived and designed, and K.K. and T.Koganezawa conducted the GIWAXD experiments. V.V., K.K. and I.O. prepared the manuscript, and all authors discussed and commented on the manuscript. V.V., I.O., K.T., and H.M. directed the project.

Supplementary Information

Efficient inverted polymer solar cells employing favourable molecular orientation

Varun Vohra,[a]* Kazuaki Kawashima,[b] Takeshi Kakara,[c] Tomoyuki Koganezawa,[d]

Itaru Osaka,[b,e]* Kazuo Takimiya,[b]* Hideyuki Murata[a]*

[a] School of Materials Science, Japan Advanced Institute of Science and Technology (JAIST), 1-1 Asahidai, Nomi, Ishikawa, 923-1292, Japan

[b] Emergent Molecular Function Research Group, RIKEN Center for Emergent Matter Science (CEMS), Wako, Saitama 351-0198, Japan

[c] Department of Applied Chemistry, Graduate School of Engineering, Hiroshima University, 1-4-1 Kagamiyama, Higashi-Hiroshima, Hiroshima 739-8527, Japan

[d] Japan Synchrotron Radiation Research Institute, 1-1-1, Kouto, Sayo-cho, Sayo-gun, Hyogo 679-5198, Japan

[e] Precursory Research for Embryonic Science and Technology, Japan Science and Technology Agency, Chiyoda-ku, Tokyo 102-0075, Japan

E-mail: varun.vohra@uec.ac.jp (V.V.), itaru.osaka@riken.jp (I.O.), takimiya@riken.jp (K.T.), murata-h@jaist.ac.jp (H.M.)

1. Photovoltaic properties of PNTz4T cells

2. Hole-only and electron-only devices

3. GIWAXD analyses

4. Photos of an DCB droplet

1. Photovoltaic properties of PNTz4T cells

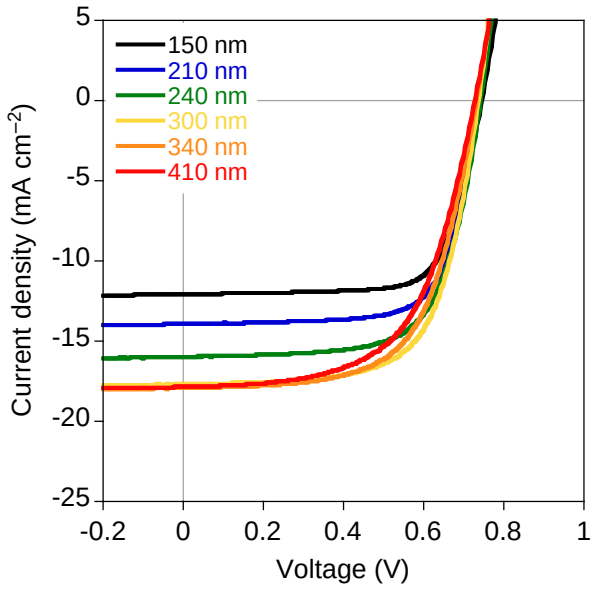

Figure S1. *J*–*V* curves of conventional cells with $PC_{61}BM$.

Table S1. Photovoltaic parameters of conventional cells with $PC_{61}BM$.

thickness (nm)	J_{SC} (mA cm^{-2})	V_{OC} (V)	FF (%)	PCE (%)
150	12.1	0.746	72.7	6.55
210	13.9	0.739	71.5	7.36
240	16.0	0.743	67.9	8.06
300	17.7	0.738	66.7	8.70
340	17.9	0.732	63.2	8.30
410	17.9	0.729	59.8	7.78

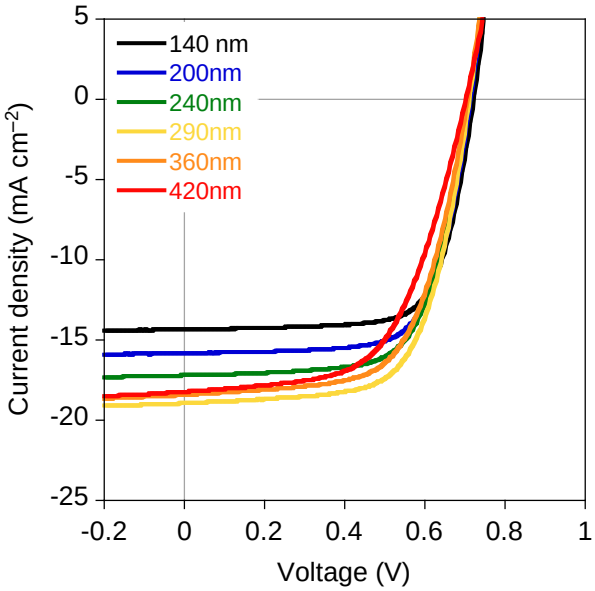

Figure S2. *J*–*V* curves of conventional cells with $PC_{71}BM$.

Table S2. Photovoltaic parameters of conventional cells with $PC_{71}BM$.

thickness (nm)	J_{SC} (mA cm^{-2})	V_{OC} (V)	FF (%)	PCE (%)
140	14.3	0.723	72.1	7.47
200	15.8	0.715	70.0	7.92
240	17.2	0.711	67.6	8.27
290	18.9	0.712	66.2	8.92
360	18.4	0.708	63.8	8.31
420	18.2	0.703	58.6	7.51

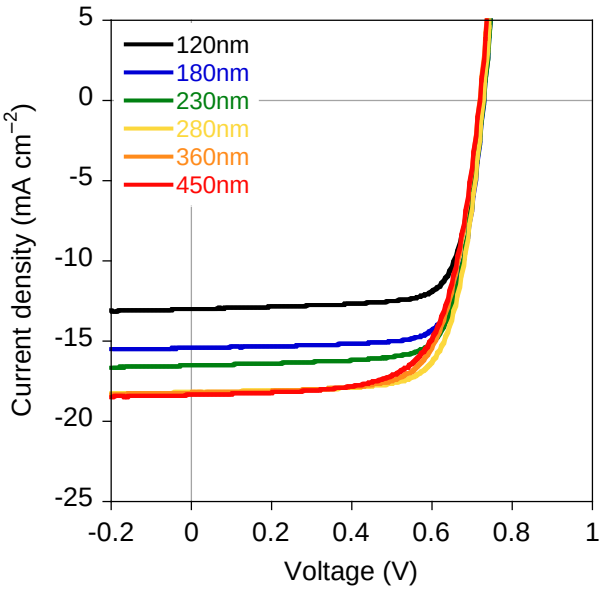

Figure S3. *J*–*V* curves of inverted cells with $PC_{61}BM$.

Table S3. Photovoltaic parameters of inverted cells with $PC_{61}BM$.

thickness (nm)	J_{SC} (mA cm^{-2})	V_{OC} (V)	FF (%)	PCE (%)
120	13.0	0.725	76.2	7.18
180	15.4	0.731	76.6	8.64
230	16.5	0.730	75.2	9.07
280	18.2	0.729	73.9	9.80
360	18.2	0.719	71.5	9.37
450	18.4	0.720	68.7	9.08

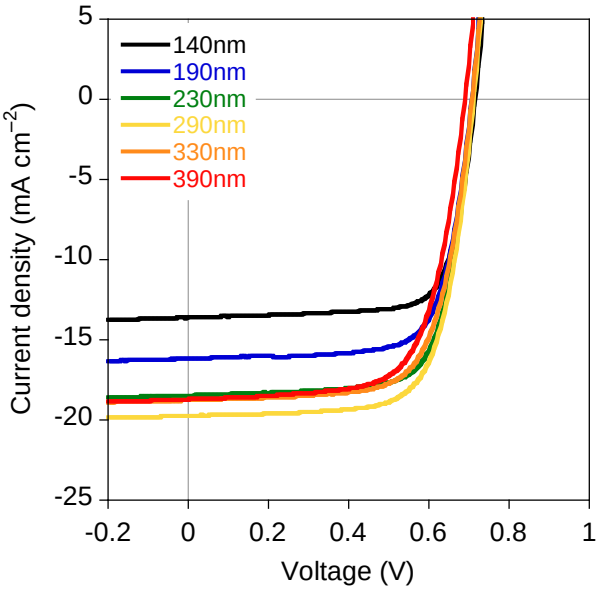

Figure S4. *J*–*V* curves of inverted cells with $PC_{71}BM$.

Table S4. Photovoltaic parameters of inverted cells with $PC_{71}BM$.

thickness (nm)	J_{SC} (mA cm^{-2})	V_{OC} (V)	FF (%)	PCE (%)
140	13.6	0.716	75.1	7.33
190	16.2	0.708	73.1	8.36
230	18.5	0.712	72.8	9.57
290	19.4	0.708	73.4	10.1
330	18.8	0.708	70.1	9.32
390	18.7	0.691	68.4	8.84

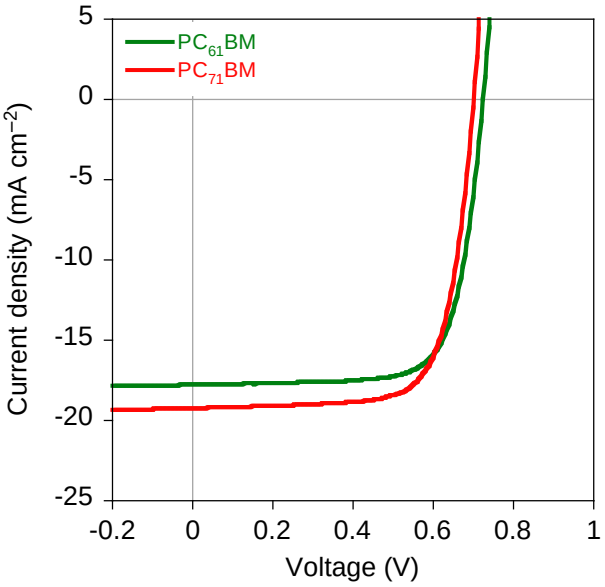

Figure S5. *J*–*V* curves of inverted cells (area: 0.16 cm^2) measured using a photomask with a 0.1225 cm^2 aperture.

Table S5. Photovoltaic parameters of inverted cells using a photomask.

PCBM	thickness (nm)	J_{SC} (mA cm^{-2})	V_{OC} (V)	FF (%)	PCE (%)
$PC_{61}BM$	340	17.8	0.725	74.3	9.58
$PC_{71}BM$	290	19.2	0.703	73.4	9.90

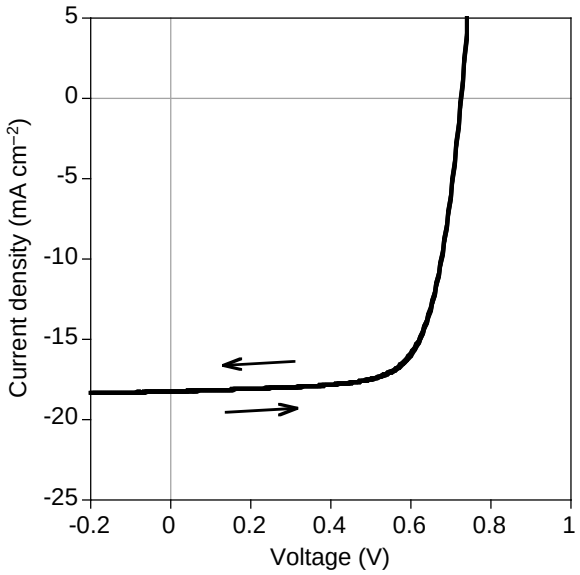

Figure S6. *J*–*V* curves of a inverted PNTz4T/$PC_{61}BM$ cell at forward and reverse sweeps

Table S6. Photovoltaic parameters of a inverted PNTz4T/$PC_{61}BM$ cell at forward and reverse sweeps

Sweep direction	J_{SC} (mA cm^{-2})	V_{OC} (V)	FF (%)	PCE (%)
forward	18.2	0.726	72.5	9.60
reverse	18.3	0.727	72.3	9.59

Reference No. 14TR-PV0022

Measurement Report

Client Name	RIKEN
Client Address	2-1 Hirosawa, Wako, Saitama 351-0198
Measurement Items	Organic solar cell
Manufacturer	RIKEN
Type	PNTz4T/PC$_{71}$BM
Serial Number	141120
Application number	C14R0025
Application date	20 Nov 2014
Measurement method	IEC60904-1ed.2, JIS C 8913(2005), JIS C 8915(2005)
Measurement Location	JAPAN ELECTRICAL SAFETY & ENVIRONMENT TECHNOLOGY LABORATORIES DIRECTOR OF RESEARCH AND BUSINESS DEVELOPMENT 1-12-28 MOTOMIYA TSURUMI-KU YOKOMAHA KANAGAWA, 230-0004 JAPAN
Measurement date	20 Nov 2014
Measurement Authority	Takamitsu Inoue

Issued date
16 Dec 2014

Approved By
Director of Research and Business Development
Eiji Yamada

JAPAN ELECTRICAL SAFETY & ENVIRONMENT TECHNOLOGY LABORATORIES
1-12-28 MOTOMIYA TSURUMI-KU YOKOMAHA KANAGAWA, 230-0004 JAPAN

The Measurement Result presented in this report is valid only for the module measured.
The Measurement Report shall not be reproduced without the written approval of JET.

I-V CURVE

JIS C 8913-2005/IEC60904-1-2006Ed.2 YSS-200AA
Total area 0.1220 cm²(submitted by RIKEN)

CURRENT [mA]
POWER [mW]
VOLTAGE [V]
CURRENT
POWER

Date:	2014/11/20
Type:	PNTz4T/PC$_{71}$BM
Sample No.:	141120
Repeat Times:	3
Isc:	2.195 [mA]
Voc:	0.708 [V]
Pmax:	1.120 [mW]
Ipmax:	1.960 [mA]
Vpmax:	0.571 [V]
Eff.:	9.2 [%]
F.F.:	72.0 [%]
M.Temp.	25.0 [°C]
R.Temp:	25.0 [°C]
Irr.:	1012 [W/m^2]

Figure S7. Datasheet for characterization of a inverted PNTz4T/PC$_{71}$BM cell at Japan Electrical Safety & Environment Technology Laboratories (JET). The active area of the cell was measured at National Institute of Advanced Industrial Science and Technology (AIST).

2. Hole-only and electron-only devices.

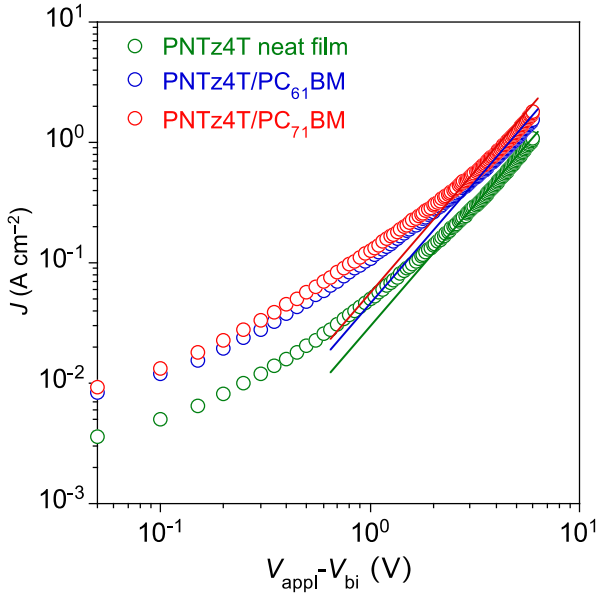

Figure S8. *J*–*V* curves of the hole-only devices (ITO/PEDOT:PSS/active layer/MoO_x/Ag).

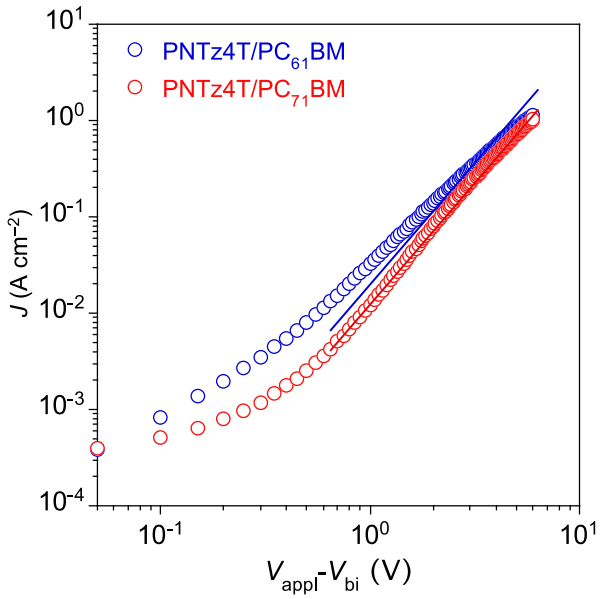

Figure S9. *J*–*V* curves of the electron-only devices (ITO/ZnO/active layer/LiF/Al).

3. GIWAXD analyses

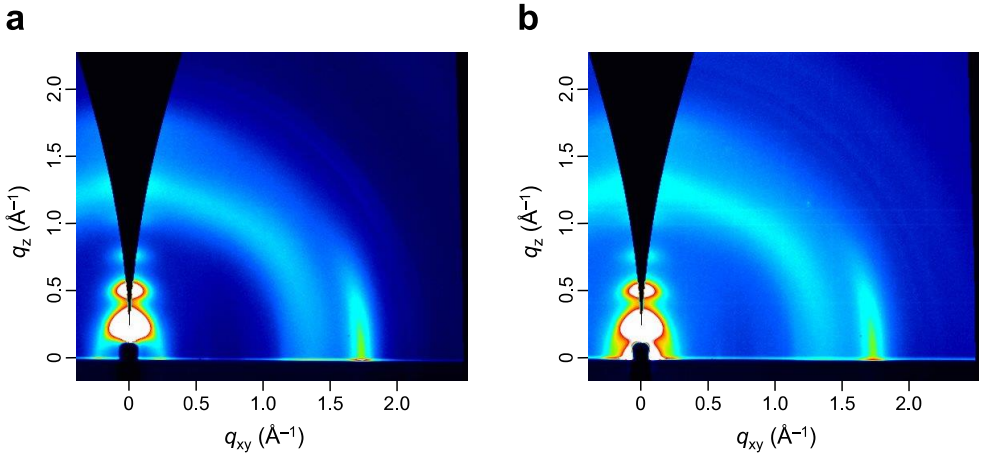

Figure S10. 2D GIWAXD patterns of the PNTz4T neat films.

(a) ITO/PEDOT:PSS substrate. (b) ITO/ZnO substrate.

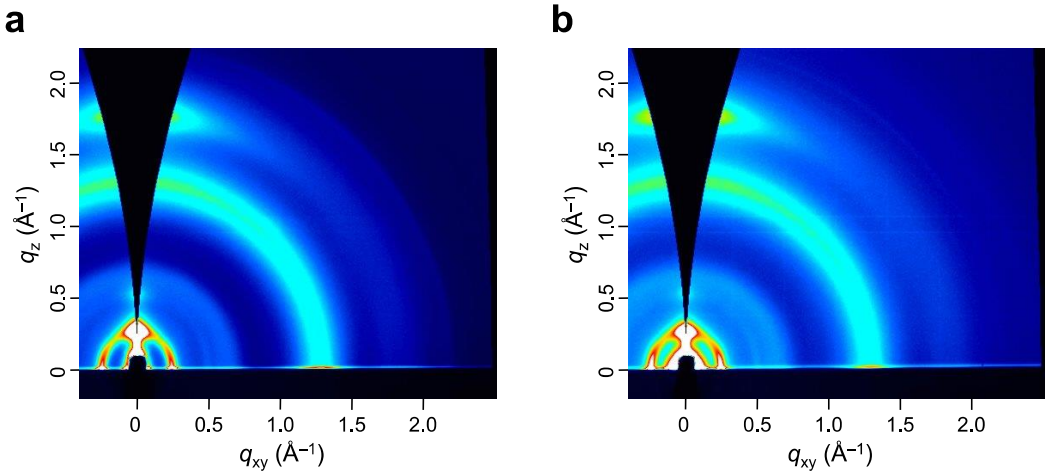

Figure S11. 2D GIWAXD patterns of the PNTz4T/$PC_{71}BM$ film (1:2 wt ratio).

(a) ITO/PEDOT:PSS substrate. (b) ITO/ZnO substrate.

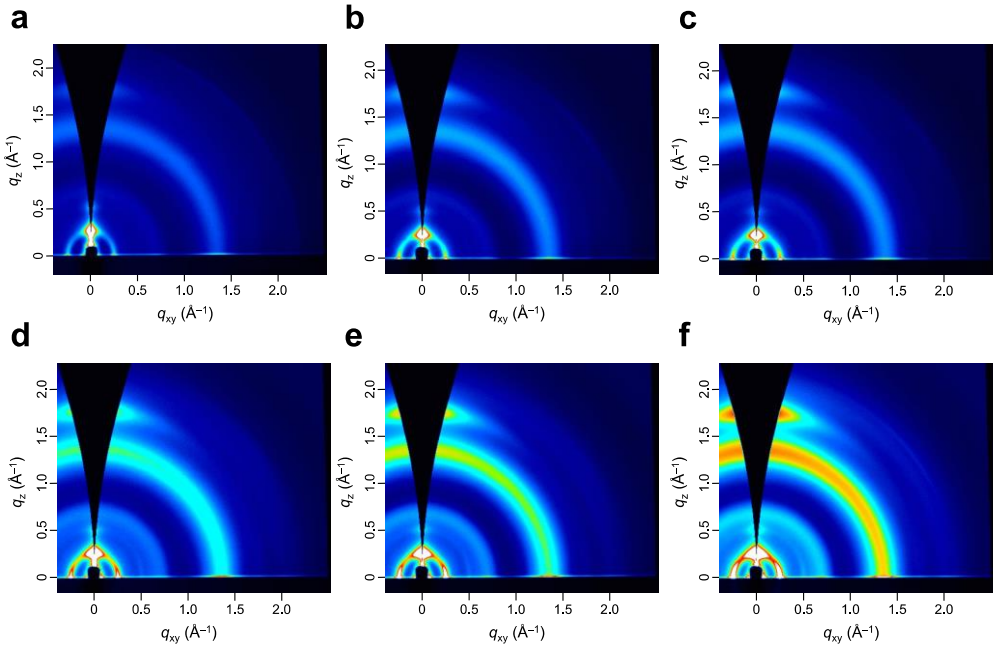

Figure S12. 2D GIWAXD patterns of PNTz4T/$PC_{61}BM$ films (1:2 wt ratio) on the ITO/PEDOT:PSS substrate. (a) 82 nm, (b) 103 nm, (c) 152 nm, (d) 241 nm, (e) 297 nm, (f) 430 nm.

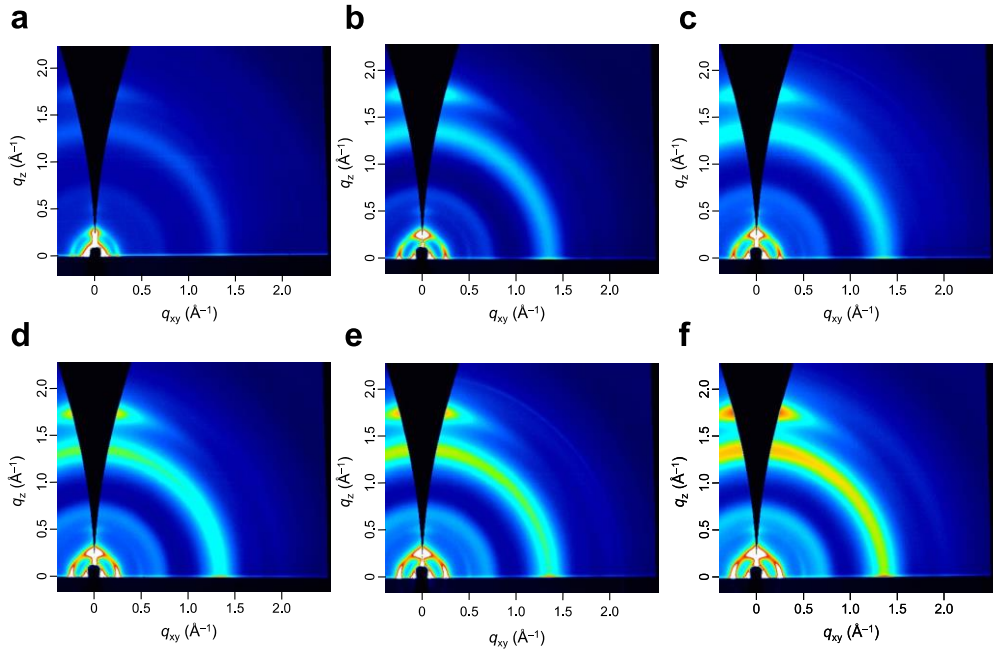

Figure S13. 2D GIWAXD patterns of PNTz4T/$PC_{61}BM$ films (1:2 wt ratio) on the ITO/ZnO substrate. (a) 46 nm, (b) 138 nm, (c) 175 nm, (d) 246 nm, (e) 297 nm, (f) 408 nm.

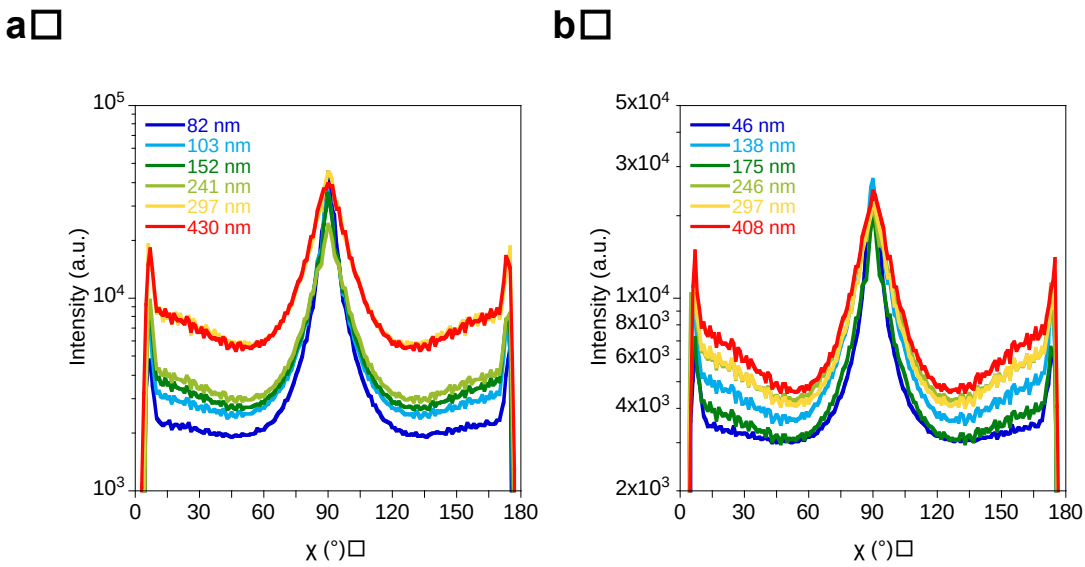

Figure S14. Pole figures of the PNTz4T/$PC_{61}BM$ films (1:2 wt ratio) with different film thickness. (a) ITO/PEDOT:PSS substrate. (b) ITO/ZnO substrate.

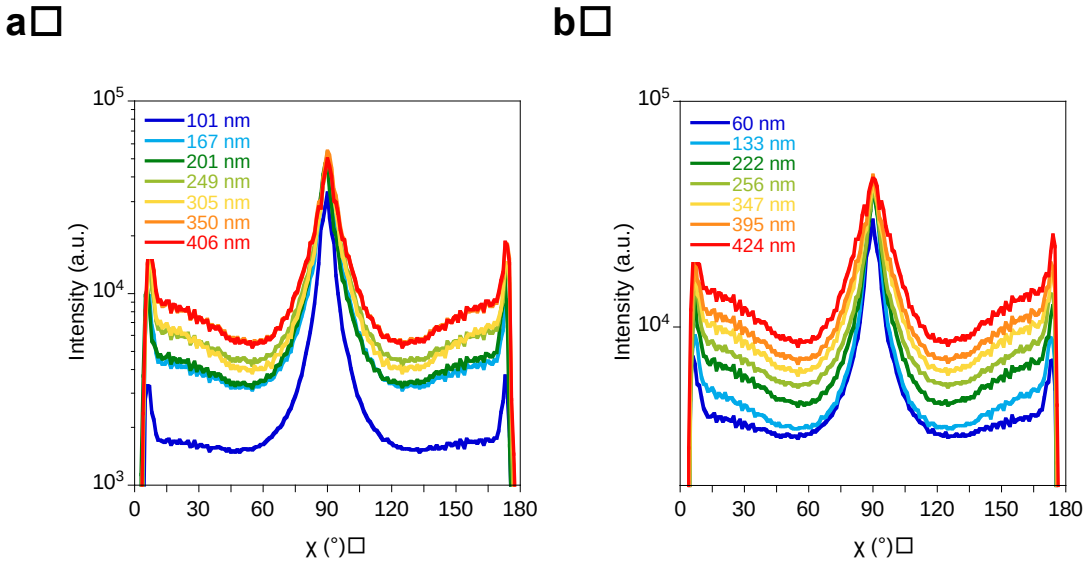

Figure S15. Pole figures of the PNTz4T/$PC_{71}BM$ films (1:2 wt ratio) with different film thickness. (a) ITO/PEDOT:PSS substrate. (b) ITO/ZnO substrate.

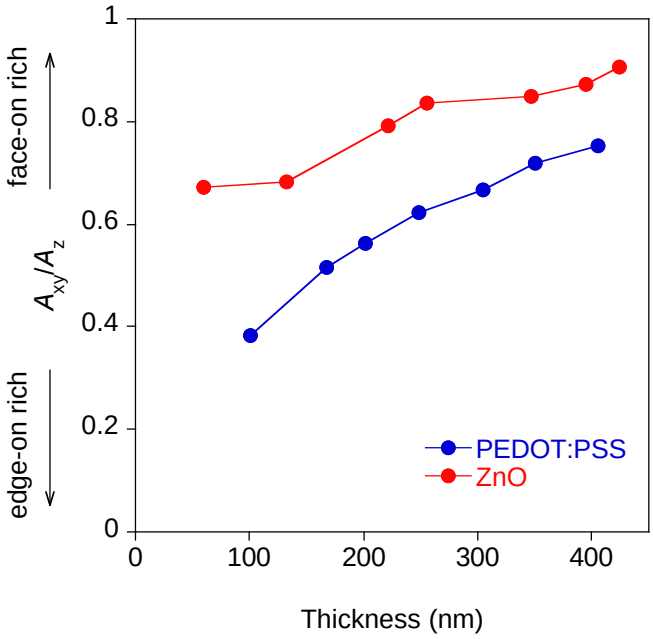

Figure S16. Dependence of A_{xy}/A_z on the film thickness for PNTz4T/$PC_{71}BM$ films

4. Contact angle measurement

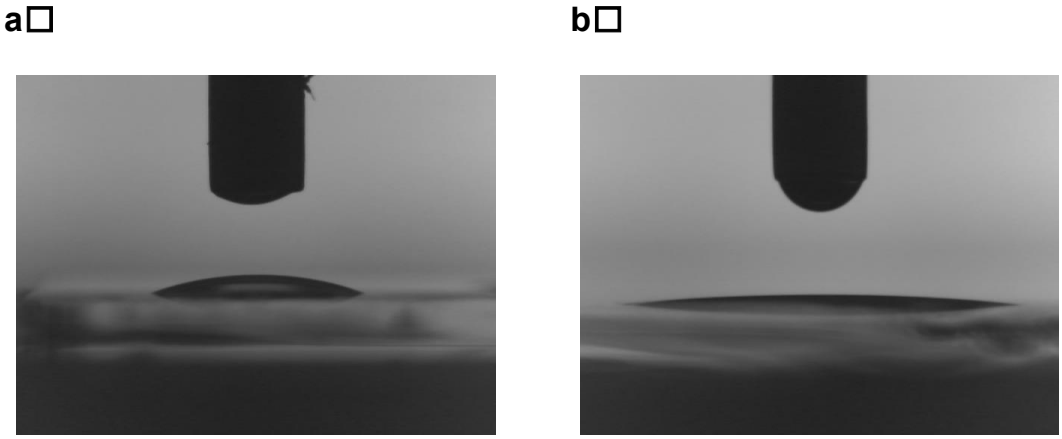

Figure S17. Photos of a DCB droplet. (a) ITO/PEDOT:PSS substrate. (b) ITO/ZnO substrate. The average contact angle of DCB, collected from 10 different substrates, on the ITO/PEDOT:PSS and ITO/ZnO substrates are 18.5° (±2.31) and 6.1° (±0.42), respectively.

5. Atomic Force Microscopy (AFM) of the PNTz4T/PCBM blend films

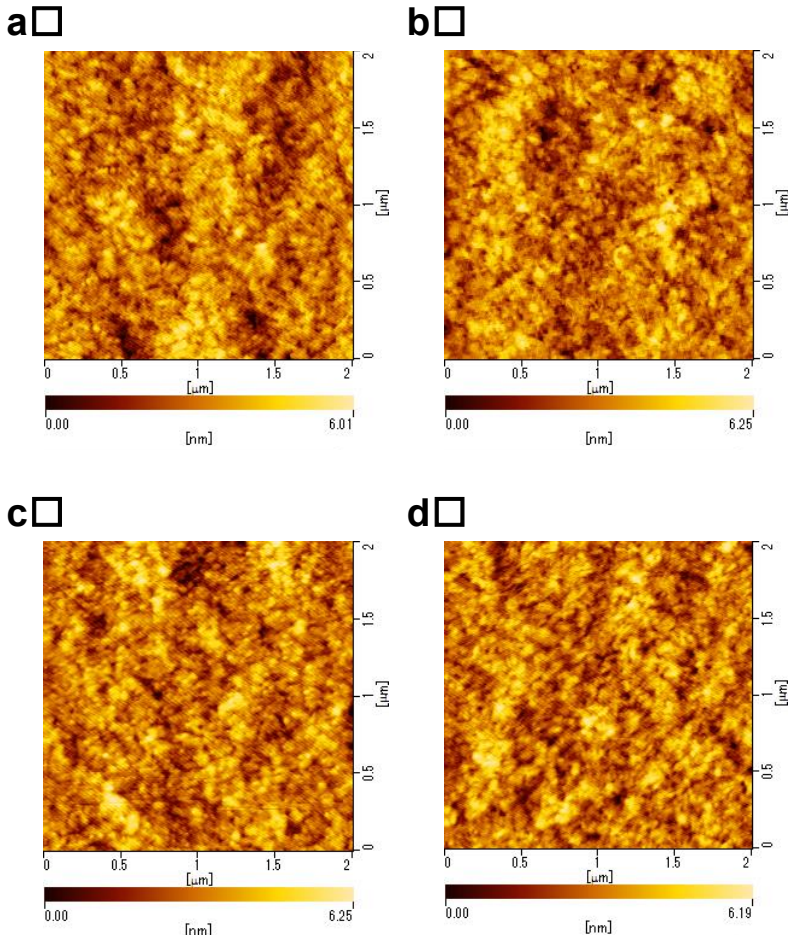

Figure S18. AFM images of PNTz4T/PCBM blend films (1:2 wt ratio). (a) PNTz4T/PC_{61}BM blend film on the ITO/PEDOT:PSS substrate. (b) PNTz4T/PC_{71}BM blend film on the ITO/PEDOT:PSS substrate. (c) PNTz4T/PC_{61}BM blend film on the ITO/ZnO substrate. (d) PNTz4T/PC_{71}BM blend film on the ITO/ZnO substrate. The AFM study was carried out with the dynamic force mode measurement by using a Nanocute scanning probe microsope system (SII Nanotechnology, Inc.).

6. Cross-sectional EDS mapping profiles and images of the PNTz4T cells

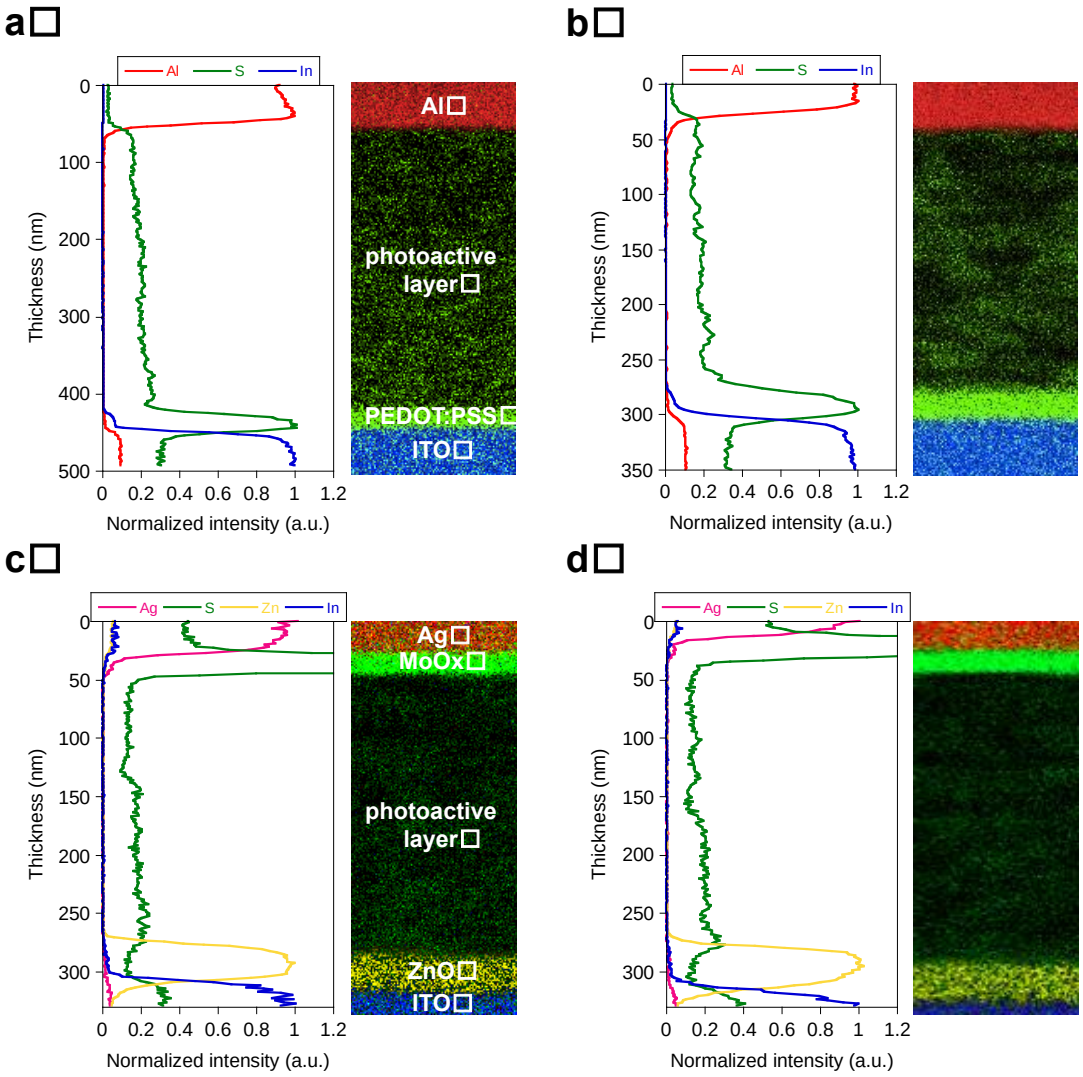

Figure S19. Cross-sectional EDS mapping profiles (left) and images (right) for PNTz4T cells. (a) $PC_{61}BM$ conventional cell. (b) $PC_{71}BM$ conventional cell. (c) $PC_{61}BM$ inverted cell. (b) $PC_{71}BM$ inverted cell.